EurJOC
European Journal of Organic Chemistry

Research Article
doi.org/10.1002/ejoc.202400914

Chemistry Europe
European Chemical Societies Publishing

www.eurjoc.org

Design and Synthesis of Multipath Compact Cyclophanes for Quantum Interference Studies

Salome L. Heim,[a] Almudena Gallego,[a] Valeria Bertozzi,[a] Sebastiaan van der Poel,[b] Luca Ornago,[b] Alessandro Prescimone,[a] Herre S. J. van der Zant,*[b] and Marcel Mayor*[a, c, d]

To investigate interference phenomena and conductance properties in mechanically controlled break junctions (MCBJs), macrocycles **1** and **2** (BMCs: for BenzeneMacroCycles), containing a *meta*-substituted benzene moiety with solubilizing *tert*-butyl groups, as well as structures **3** and **4** (TMCs: for ThiopheneMacroCycles), featuring 2,5-connected 3,4-hexyl-thiophene corners, were synthesized. Macrocycles **1** and **2** respectively **3** and **4** differ in the positions of the acetyl-protected sulfur anchoring groups, which impacts both, the individual transport efficiency of their parallel electronic pathways and their overall molecular wire lengths. All macrocycles were synthesized based on a series of *Sonogashira* cross-coupling reactions. For **3** and **4**, a 2-(4-pyridinyl)ethyl protecting group for the sulfur atoms was successful, while for macrocycles **1** and **2** the more common *tert*-butyl protecting group did the job. To our delight, proof-of-concept charge transport studies conducted in an MCBJ setup demonstrated the expected trends regarding improved conductance intensities for the TMCs compared to the BMCs. Furthermore, the corresponding molecular plateaus from the breaking experiments were in the expected length range of the S–S distances for all compounds. We also found that the overall conductance seems to follow a more complex transport mechanism than just the sum of contributions from both channels.

Introduction

Interference phenomena in single molecular junctions are of fundamental interest, as they provide an opportunity to integrate particular functions into the junction by molecular design.[1–12] Already very basic theoretical considerations rationalized the large difference in transport properties between *para*- and *meta*- benzene as constructive and destructive interference respectively of a pair of transport channels.[13–17] Interference features were predicted for and realized in molecular junctions comprising delocalized π-systems,[11,18–22] the latter separated either by sp^3 hybridized[23] or geminally integrated sp^2 hybridized carbon atoms,[24,25] rigid silicon based bicyclic structures,[26] or small cyclic structures.[27] The phenomenon moved recently even more into the focus of interest, as promising thermoelectrical features were predicted.[28–30] Impressive conductance switching in molecular junctions was reported by oxidizing conjugated hydroxy substituted π-systems into the corresponding quinone forms with considerably reduced transparency due to destructive interference.[11,31,32] A destructive interference dip was observed in pseudo-*para* [2.2] cyclophanes, giving molecules comprising this subunit impressive mechano sensitivity properties.[33,34] Surprisingly, very comparable features arising from interference phenomena were also obtained for larger porphyrin cyclophanes.[35,36]

Interference phenomena can be observed at the merging point of two (or more) wave-type signals, where their amplitudes add up or cancel. In a quantum mechanical description, also electrical currents are described as waves, and thus their interference was theoretically predicted[37] and experimentally demonstrated in mesoscopic physics.[38] Usually a few hundred nm sized split rings were used to separate the electrical current into two parallel pathways,[39] manipulated by external triggers like e.g. the applied magnetic field. Macrocyclic molecular structures resemble the split ring design of mesoscopic physics and are thus particular appealing as potential candidates to produce interference phenomena in single molecule junctions. However, their considerable smaller dimension (a few nm) makes the manipulation of both parallel pathways by applied magnetic fields much more challenging. As an alternative approach, the electronic transparency of both parallel channels can be manipulated by molecular design, i.e., by the choice of connectivity patterns in the subunits. The subsequent comparison of the transport features between structurally comparable macrocycles can then be discussed in terms of interference contributions.

[a] S. L. Heim, A. Gallego, V. Bertozzi, A. Prescimone, M. Mayor
Department of Chemistry, University of Basel, St. Johanns-Ring 19, Basel CH-4056, Switzerland
E-mail: marcel.mayor@unibas.ch

[b] S. van der Poel, L. Ornago, H. S. J. van der Zant
Kavli Institute of Nanoscience, Delft University of Technology, GA Delft 2600, The Netherlands
E-mail: h.s.j.vanderzant@tudelft.nl

[c] M. Mayor
Institute for Nanotechnology (INT), Karlsruhe Institute of Technology (KIT), Karlsruhe D-76021, Germany

[d] M. Mayor
Lehn Institute of Functional Materials (LIFM), School of Chemistry, Sun Yat-Sen University (SYSU), Guangzhou 510275, China

Supporting information for this article is available on the WWW under https://doi.org/10.1002/ejoc.202400914

Research Article
doi.org/10.1002/ejoc.202400914

Here, the synthesis and first single molecule transport investigations of two small series of macrocycles with a pair of parallel conduction paths are presented. Figure 1 displays the four macrocyclic model compounds together with the intended transport channels as arrows. The electronic transparency of the individual conduction channel is varied by the connectivity within the interlinked aryl systems. The model compounds **1** and **2** of the first series consist exclusively of ethynyl interlinked benzene subunits, while both central benzene subunits have been replaced by thiophenes in **3** and **4** of the second series. In one of the very first systematic single molecule transport studies the large difference between a *para*- and *meta*-connection in a benzene ring was already demonstrated,[40] and corroborated by subsequent transport experiments.[12,41]

Due to the expected differences in efficiency of transport, the intention of the here presented macrocyclic model compounds is to investigate the ability to distinguish between parallel transport paths, while the systematic manipulation of interference phenomena arising from the two parallel paths are not yet in the focus of interest.

Results and Discussion

Design

Predictions about the conductance through a particular channel of a macrocyclic model compound can be made by adding up the sequential substitution patterns of the connecting corner units that are ether phenyl or thiophene derivatives. Favorable conductance features are expected for the *para* connections like 1,4-substituted benzene or 2,5-substituted thiophene due to constructive interference (displayed by a red color in the transport channels in Figure 1), while the *meta* connection of 1,3-substitution in benzene should result in less favorable transport properties due to destructive interference (highlighted by a blue color in the transport channels in Figure 1).[42] In all the four macrocyclic model compounds charge transport can occur *via* two different pathways. Macrocycles **1** and **3** have both a C_2 symmetry axis perpendicular to the plane defined by both, the macrocycle and the plane on which it is drawn. As a consequence, both bear two connectivity and lengthwise similar pathways. In contrast to that, the macrocycles **2** and **4** have both two pathways with different sequences of connecting patterns and over-all length for charge transport. Based on the *para vs meta*-arguments mentioned above, the replacement of the 1,3-connected benzene corner (**1** and **2**) by a 2,5-connected thiophene subunit (**3** and **4**) is expected to improve the transport features of the respective channel, while a suitable angle for macrocyclization is maintained.

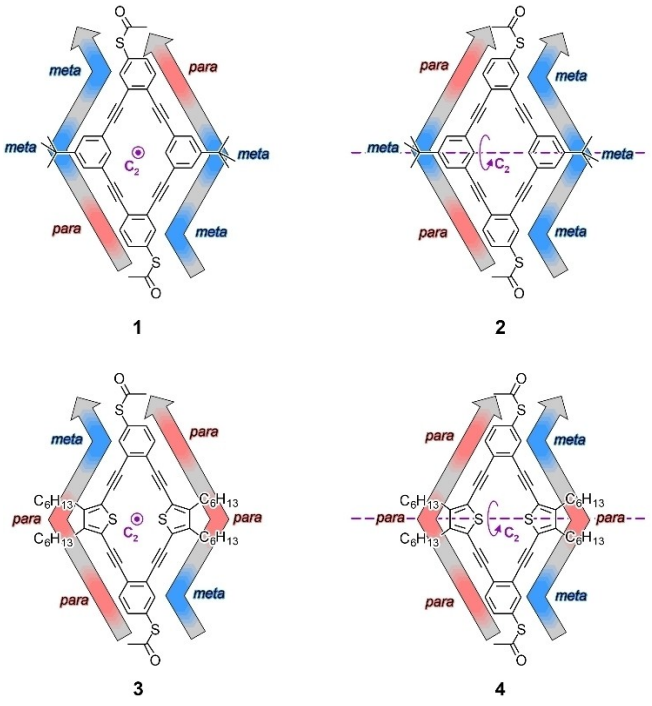

Figure 1. Target macrocycles **1**–**4** with intended current paths indicated by arrows. The colour code displays the expected transport qualities of the joints with red as electronically more transparent *para*-connection and blue as less transparent *meta*-connection. The C_2 symmetry axis of each molecule is displayed in lila.

Predictions about the order of the conductance between the four macrocycle model compounds **1**–**4** are more challenging, as it remains unknown how pairs of similar transport channels add up. Only considering the most favourable transport channel, the best conductance would be expected for compound **4** with a channel comprising exclusively *para*-connections, followed by macrocycle **3** and **2**, each with at least one channel constructed of two *para*- and one *meta*-connection. However, while compound **3** has two of those favorable channels in parallel, it will be interesting to see to what extend it outperforms compound **2** with a single channel with only one *meta*-connection. A similar argument applies for compound **1**, with two similar and parallel channels which both comprise two *meta*- and one *para*-connection.

Forecasts are further handicapped as the substitution of a benzene corner by a thiophene not only alters the connection pattern. Both corner subunits differ in their electron density, and heteroatom effect and decreased aromaticity are known for thiophenes.[58,59] While all these features impact the conductivity features of a channel, the main focus of the here reported study is set on substitution patterns and their concomitant geometries enabling the macrocyclic structures.

Furthermore, even predictions comparing exclusively the macrocycles consisting of chemically similar corner units **1** and **2**, respectively **3** and **4** are impossible, since the mechanisms involved with interference of two different pathways is not fully understood yet. In one reported example of conductance measurement of multiple pathway macrocycles[43] a superposition law was established claiming that the total conductance is higher than the sum of the individual contributions of the pathways. In another example addition of more channels led to effective suppression of charge transport.[44]

Research Article
doi.org/10.1002/ejoc.202400914

Retrosynthesis

The challenge that accompanies the synthesis of these macrocycles consisting of subunits only differing in their substitution patterns arises from the two unalike types of symmetry that they possess. While structures **1** and **3** exhibit point symmetry with a C_2 axis pointing into the macrocyclic plane, the C_2 axis of **2** and **4** lies within the plane, as can be seen in Scheme 1. For structures **1** and **3** this means they can be synthesized over a dimerization reaction *via Sonogashira* type cross-coupling of iodo and acetylene decorated precursors **9a-c**. Macrocyclizations by dimerizations are particular appealing, as the use of a single precursor does not require perfect control over stoichiometry. The thiol anchor groups of the final macrocycles **1**–**4** are masked with labile acetyl groups which efficiently deprotect on the gold surface of the transport experiment. From a synthetic view point, the acetyl protection groups make the handling of the bifunctional macrocycles much easier, as dimerization and even polymerization reactions expected for the free thiols by disulfide formation is excluded.[45] Thus, in the retrosynthetic plan, a final transprotection step is involved to yield the target macrocycle. **9a-c** can be synthesized *via* a statistical *Sonogashira* cross-coupling involving an excess of the diiodoaryl species **6a** or **6b** and 1 equivalent of acetylenes **5a** or **5c** followed by a triisopropylsilyl (TIPS) deprotection to give the corresponding terminal acetylenes.

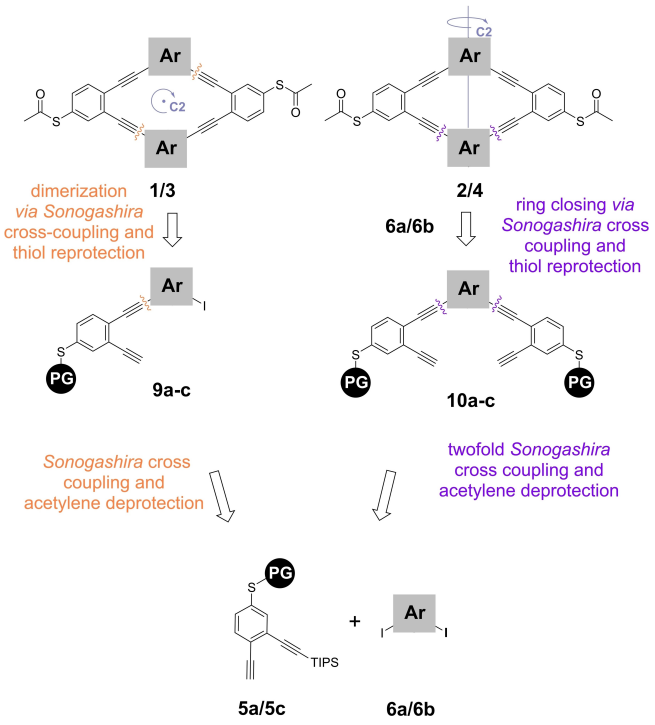

Scheme 1. Retrosynthetic strategy towards macrocyclic target structures of different symmetry assembled from the same precursors. In spite of the difference in symmetry, both strategies consist of sequential *Sonogashira* cross-couplings, TBAF deprotection, macrocyclizations *via Sonogashira* cross coupling reaction and a final transprotection step to optimize immobilization behavior and storage properties.

Even so the macrocycles **2** and **4** cannot be obtained by a similar dimerization strategy, it can be obtained by the same building blocks. In their cases the macrocylization occurs over a twofold *Sonogashira* reaction involving a diacatylene **10a-c** and a diiodo aryl **6a** or **6b**. Interestingly, the subsequent introduction of the central aryl corner in principle also allows the assembly of macrocycles with two different central aryl subunits, giving a handle to manipulate the electron density of each transport channel individually. The precursors for the macrocyclization **10a-c** can be prepared from **6a** or **6b** and acetylenes **5a** or **5c** in a twofold *Sonogashira* cross-coupling reaction. Acetylene deprotection and sulfur transprotection steps occur in a similar fashion as in the first strategy. Due to this divergent synthesis design synthetic efforts are considerably minimized.

All required building blocks should be synthetically available in reasonable amounts. The diethynyls **5a** and **5c** can both be synthesized in four steps from commercially available starting materials. The diiodo aryl unit **6a** can be synthesized by a literature known procedure.[46] Building block **6b** can be prepared by twofold iodination of commercially available 3,4-dihexylthiophene by a modified literature procedure.[47]

Synthesis

Preparation of Protected Thiophenols 5a and 5c

The syntheses of the building blocks **5a**, **5b**, and **6b** are displayed in Scheme 2. In a nucleophilic aromatic substitution of commercially available 4-fluoro-benzaldehyde with *tert*-

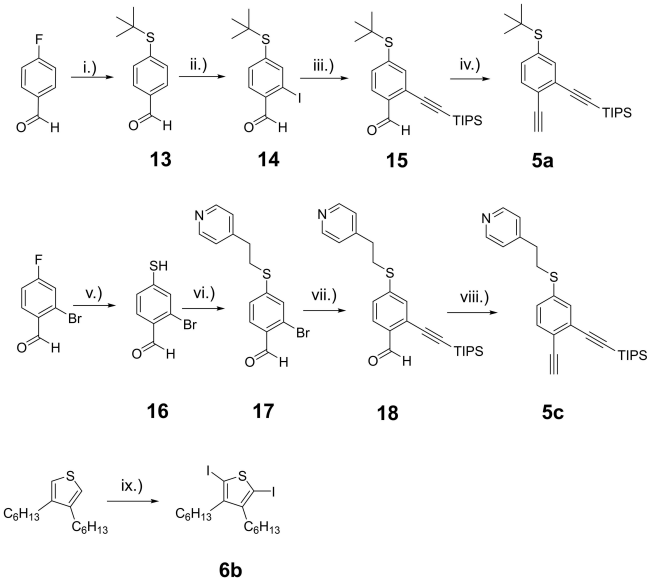

Scheme 2. i.) Cs_2CO_3, *tert*-BuSH, DMA, 90 °C, 6 h, quant.; ii.) *n*-BuLi, I_2, N,N′,N′-trimethylenediamine 33 %; iii.) TIPS-acetylene, $Pd(PPh_3)_2Cl_2$, CuI, Tol:Et_3N (10 : 1), r.t., 18 h, 92 %; iv.) Cs_2CO_3, Bestmann-Ohira reagent, MeOH, r.t., 3 h, 84 %; v.) Na_2S, DMF, r.t. 1 h; vi.) 4-vinylpyridine, toluene, 100 °C, 2.5 h, 34 % over two steps; vii.) TIPS-acetylene, $Pd(PPh_3)_2Cl_2$, CuI, Tol:Et_3N (9 : 1), r.t., 6 h, 82 %;viii). Cs_2CO_3, Bestmann-Ohira reagent, MeOH, r.t., 3 h, 47 %; ix.) NIS, PTSA, ethanol, rt, 10 min.

Research Article
doi.org/10.1002/ejoc.202400914

butylthiol in presence of Cs_2CO_3 in N,N-dimethylacetamide, **13** was synthesized in a quantitative yield, and was used without further purification. Following a modified literature procedure, an α-amino alkoxide species was formed *in situ* by addition of *n*-BuLi to a solution of N,N,N′-trimethylethylenediamine in THF at −20 °C, followed by the addition of **13.**[56] The aldehyde could be protected and a directed *ortho*-lithiation could be achieved. By trapping the aryllithium intermediate with elemental iodine, followed by aqueous work-up compound **14** was obtained in a yield of 33%. In the next step, **14** and TIPS-acetylene was engaged in a *Sonogashira* cross-coupling reaction to provide **15** in an isolated yield of 92%. **15** was converted to the terminal acetylene **5a** by applying the *Bestmann* modification of the *Seyferth Gilberth* homologation in a yield of 84%.

The two diethynyl building blocks **5a** and **5c** differ in the nature of the thiol protection group. As discussed below, the *tert*-butyl protection group turned out to be challenging in the last transprotection step for macrocycles comprising thiophene subunits, making this synthetic diversion for **3** and **4** inevitable. Thus, the reaction sequence providing building block **5c** started by treating commercially available 2-bromo-4-fluorobenzaldehyde with Na_2S in dry DMF to give the thiophenol **16**. Several attempt to isolate and purify **16** failed. Therefore, the crude mixture of **16** was directly treated with vinylpyridine to yield the sulfide **17** in a yield of 34% over both steps. **18** was obtained in 82% yield using the same reaction conditions described for **15** and was subsequently reacted to **5c** in 47% yield with a similar protocol as applied for **5a**. Compound **6a** was synthesized according to a literature protocol.[46] Diodo thiophene **6b** was synthesized *via* a PTSA-catalysed iodination using NIS from commercially available 3,4-dihexylthiophene.[47]

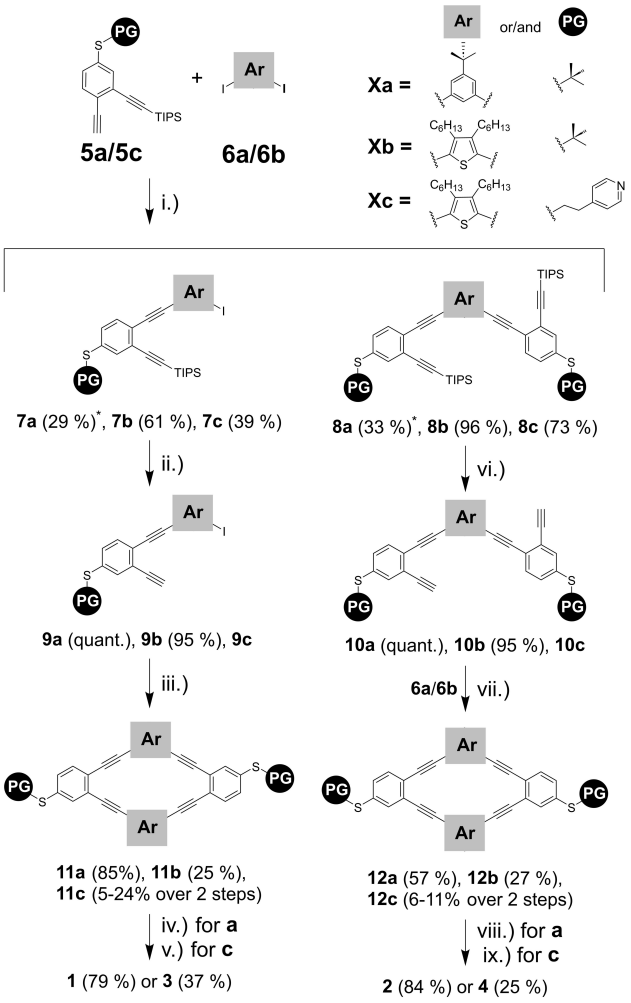

Scheme 3. Assembly of the macrocycles **1**–**4**. The chemical structures of the place holders "Ar" and "PG" are displayed in the upper right corner. Reagents and conditions: i.) **7a**/**8a**: $Pd(PPh_3)_4$, CuI, Tol/Et_3N; towards **7b**: $Pd(PPh_3)_4$, CuI, Tol/Et_3N, rt; **8b**: $Pd(PPh_3)_4$, CuI, Tol/Et_3N, 85 °C, 8 h ; **7c**/**8c**: $Pd(PPh_3)_2Cl_2$, CuI, Tol/Et_3N, rt, 8 h ii.) TBAF, THF, r.t., 30 min; iii.) **11a**: $Pd(PPh_3)_4$, Tol/Et_3N, CuI, 85 °C ; **11b**: $Pd(PPh_3)_4$, THF/Et_3N, CuI, 65 °C ; **11c**: $Pd(PPh_3)_2Cl_2$, Tol/Et_3N, CuI, 65 °C ; iv.) $Bi(OTf)_3$, Acetyl chloride, Tol/ACN (1 : 1), r.t., 1 h; v.) 1. MeI, Acetone, 20 h, rt, 2. K_2CO_3, acetic anhydride, DMF/H_2O, r.t., 3 h; vi.) TBAF, THF, r.t., 30 min; vii.) **12a**: $Pd(PPh_3)_4$, Tol/Et_3N, CuI, 85 °C ; **12b** : $Pd(PPh_3)_4$, THF/Et_3N, CuI, 65 °C ; **12c**: $Pd(PPh_3)_2Cl_2$, Tol/Et_3N, CuI, 65 °C ; viii.) $Bi(OTf)_3$, Acetyl chloride, Tol/ACN (1 : 1), r.t., 1 h; ix.) 1. MeI, Acetone, 20 h, rt, 2. K_2CO_3, acetic anhydride, DMF/H_2O, r.t., 3 h; *obtained in the same reaction, yields with respect to the diodoaryl.

Macrocycles 1 and 2 Consisting Exclusively of Phenyl Corner Units

The assembly of the macrocycles **1**–**4** from their building blocks is displayed in scheme 3.

A mixture of **7a** and **8a** were isolated from a *Sonogashira* cross-coupling of 1 eqivalent of **6a** with 1.5 equivalents of **5a** and were separated by gel permeation chromatography (GPC) to give **7a** in 29% and **8a** in 33% yields, respectively. In a next step **7a** and **8a** were deprotected with tetrabutylammonium fluoride (TBAF) to give **9a** and **10a** in quantitative yields.

The macrocycle **11a** should be obtained by a dimerization of **9a** in an intermolecular *Sonogashira* cross-coupling followed by an intramolecular one closing the macrocycle. To minimize the formation of larger cyclic and/or open chain oligomers, high dilution conditions were considered. However, macrocyclizations by *Sonogashira* reactions are challenging, as the substituted halide as well as the reacting ethynyl have both to be activated individually by a catalyst. Thus, it is not enough that both groups engaged in the coupling meet, they also have to be activated by the catalyst. As additional challenge, Pd(0) activated halides are prone to dehalogenation as competing reaction pathway.

To our delight, the dimerization of **9a** in rather high diluted (1.6 mM) conditions using 10 mol% of $Pd(PPh_3)_4$ as catalyst and 5 mol% of CuI in Toluene/Et_3N at 85 °C provided the macrocycle **11a** in excellent 85% isolated yields as orange solid. The rather high temperature, considering the fact that aryliodides engage in *Sonogashira* reactions already at room temperature, was applied with the rational to provide enough intramolecular mobility after the first interlinking of two molecules to favour intramolecular ring closing. It is noteworthy that initial attempts to add the monomer **9a** dropwise to the reaction mixture comprising the catalytic system were not successful. It seemed that in such "pseudo high dilution" condition dehalogeniation was favoured over macrocyclization.

Research Article
doi.org/10.1002/ejoc.202400914

While the macrocycle **11a** was accessible by a dimerization of **9a** exposing both, an iodine and an ethynyl group, the macrocyclization of **12a** should be obtained by the twofold *Sonogashira* coupling between two bifunctional building blocks, the diethynyl **10a** and the diiodide **6a**. Control over the stoichiometry is crucial for the macrocyclization based on two different bifunctional precursors. Thus, equimolar amounts of excessively purified precursors **10a** and **6a** were exposed to similar reaction conditions as described above for the assembly of **11a**, with the minor variation that the concentration of both precursors was set to 1.4 mM. The macrocycle **12a** was obtained in 57% isolated yield.

In the final transprotection reaction transforming the S-*tert*-butyl protected macrocycles **11a** and **12a** to the S-acetyl masked target structures **1** and **2**, the precursors **11a** and **12a** were exposed to bismuth(III) trifluoromethanesulfonate in presence of acetyl chloride, to provide the target macrocycles **1** and **2** in 79 and 84% isolated yield respectively as yellow solids.

Macrocycles 3 and 4 Comprising Thiophene Subunits

As the syntheses of the macrocycles **1** and **2** were successful, the intention was to assemble **3** and **4** by the same synthetic strategy. The statistical *Sonogashira* cross-coupling between **5a** (8.2 mM) and 10.5 equivalents of diodoaryl **6b** gave **7b** in a yield of 61%. A change of solvent from toluene to THF was made since better results were observed with these conditions, presumably due to better ligand dissociation from $Pd(PPh_3)_4$ to the catalytically active Pd(0) species in a coordinative solvent. Also, competitive coordination of the thiophene subunits to the Pd is less likely in this solvent system. Deprotection of the acetylene with TBAF afforded **9b** in an excellent yield of 95%. High dilution (1.5 mM) dimerization of **9b** over a twofold *Sonogashira* cross-coupling in THF/Et_3N, CuI (46 mM) and Pd-$(PPh_3)_4$ (20 mM) as catalysts at 65 °C yielded macrocyle **11b** in a yield of 25% after purification by GPC as a yellow solid. Macrocyclization pecursor **10b** was prepared in a twofold *Sonogashira* cross coupling with 2.1 equivalents of **5a** and **6b** at 85 °C to give **8b** in 96% yield followed by deprotection with TBAF. An equimolar mixture of **10b** and **6a** were reacted under high dilution (1.7 mM) under similar reaction conditions as decribed for the previous macrocyle to give **12b** in a yield of 27% as a yellow solid.

Comparing these macrocyclizations to the previous ones resulting in **11a** and **12a**, a substantial drop in the isolated yields was observed. As potential explanations either the coordination of the catalyst to the thiophene sulfur or a less favored spatial arrangement for the ring closing of the dimer after the first coupling reaction were hypothesized.

Unfortunately, all attempts to convert **11b** and **12b** to the acetyl protected macrocycles **3** and **4** failed. Exposed to the transprotection conditions previously providing **1** and **2** the precursor macrocycles **11b** and **12b** were consumed, but the formation of **3** and **4** was not observed. Most likely faster side reactions with the *Lewis* acidic reagents made this transformation impossible.

At this point we became aware that a different type of masking group for the thiophenol is required, namely one that can selectively be de- or trans- protected without interfering with the functional subunits of the macrocyclic core. As alternative protection group 2-(4-pyridinyl)ethyl was considered. After assembly of the macrocyclic structures, the C–S bond can be cleaved under basic conditions after alkylation of the pyridyl moiety. The alkylation results in a charged species and an increase of the acidity of the β hydrogen atoms. The subsequent addition of a base leads to the formation of the deprotected species and vinyl pyridine. The strategy has previously been applied for similar multi-step reactions[48,49] including *Sonogashira* cross-couplings and acetylene deprotections and originates from the pioneering work of *Katritzky* and co-workers in 1984. Interestingly, the method is not exclusive for masking thiols, but works also for carboxylic acids and sulfinic acids.[50] Fortunately, our initial concerns of exposing pyridyl subunits during the assembly of the macrocycle, which might coordinate the Pd catalyst or enhance the chromatographic challenges due to increased polarity, turned out to be not justified.

Variation of the Protection Groups of the Thiophenols

The assembly of the macrocycles **11c** and **12c** was in large an optimization of the protocols developed for **11b** and **12b**. In analogy to the assembly of **7a** and **8a**, the statistical *Sonogashira* cross-coupling of **5c** with **6b** gave best results with toluene as solvent at room temperature. The Pd(0) catalyst was prepared in-situ with $Pd(PPh_3)_2Cl_2$ as palladium source. To avoid the requirement of a large excess of **6b**, a pseudo high dilution strategy was applied where a degassed solution of **5c** in toluene was slowly dropped to the reaction mixture comprising **6b**. The method provided **7c** in yields up to 49%, while attempts using large excesses of diiodo aryl gave only yields between 20 and 40%. The dimerization precursor **9c** comprising an ethylpyridine masked thiol was obtained by treating **7c** with TBAF. The crude of the deprotection reaction was directly used for the next step. For the Macrocyclization reaction towards **11c**, similar *Sonogashira* cross-coupling conditions as discussed before for the assembly of its precursors were applied with an increased temperature of 65 °C. Using rather high dilution conditions (1.2 mM), the desired macrocycle **11c** was obtained as yellow oil in isolated yields varying between 5 and 24% over two steps. Unfortunately, isolated yields dropped with increasing scale of the macrocyclization reaction.

The precursor **8c** was isolated in a yield of 73% in a twofold *Sonogashira* cross-coupling of **6b** and 2.2 equivalents of **5c** applying similar reaction conditions as already described for **7c**, without the pseudo high dilution strategy. Deprotection of **8c** with TBAF gave **10c**, which was directly used together with one equivalent of **6b** for high dilution (3.3 mM) *Sonogashira* macrocyclization. The macrocycle **12c** was isolated in yields between 6–11% over both steps as yellow oil. In similarity to **11c**, again dropping yields with increasing scale of the reaction were

Research Article
doi.org/10.1002/ejoc.202400914

observed. To separate the target structure from dehalogenated side products and open chain oligomers, size exclusion chromatography on SX3 BioBeads® was performed.

The substantial drop in yield in the macrocyclization from **11a** (85%) and **12a** (57%) over **11b** (25%) and **12b** (27%) to **11c** (5–24%) and **12c** (6–11%), we rationalize with the increasing number of coordination sites in the structures which might interfere with the catalytically active metals in the *Sonogashira* cross coupling reaction.

Finally, the target macrocycles **3** and **4** were obtained from their corresponding 2-(4-pyridinyl)ethyl protected precursors **11c** and **12c** *via* a three-step transprotection protocol. First the pyridine groups were methylated using methyl iodide (MeI) in acetone at room temperature. After removing solvent and remaining reagents under reduced pressure, the crude methyl pyridinium iodides were then treated with K_2CO_3 in DMF and water in the second step to liberate the thiophenols. Direct addition of acetic anhydride to the reaction mixture gave the acetylated target structure **3** and **4** as yellow solids, with isolated yields of 36 and 25% respectively over all three steps. Removal of any residual methyl iodide after the first step turned out to be crucial, as otherwise immediate methylation of the thiophenol was observed in the basic environment.

All new compounds were fully characterized by ^{1}H-NMR and ^{13}C-NMR spectroscopy as well as high resolution electron spray ionization mass spectrometry (ESI-MS), except for macrocycles **11b** and **12b** which were characterized using a matrix-assisted laser desorption/ionization source for the time of flight mass spectrometer (MALDI-ToF-MS). In addition, single crystals suitable for x-ray diffraction analysis were obtained for macrocycle **1** by slow evaporation of a CH_2Cl_2 solution. The procedure provided orange needles which fortunately were thick enough for the diffraction experiment.

The macrocycle crystallizes in the *P*-1 point group and its solid state structure is displayed in figure 2a.) and b.). The entire compact macrocycle is almost planar, at least within the crystal lattice. A particular interesting value for the intended transport experiments is the sulfur to sulfur distance of 1.75 nm.

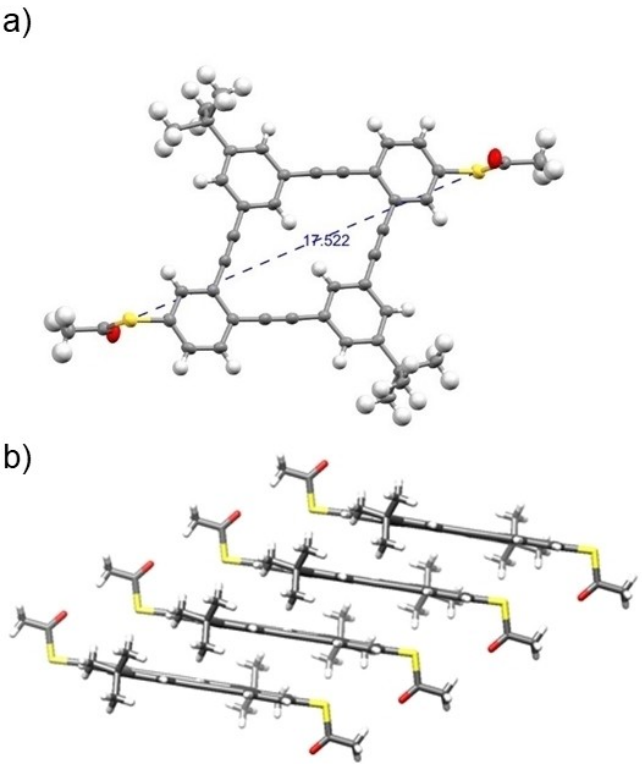

Figure 2. Solid state structure of macrocycle **1**. a) ORTEP plot of the structure with 50% probability providing the sulfur to sulfur distance of 1.75 nm. b) The parallel planes packing of the macrocycle in the crystal.

Charge-Transport Studies

Charge-transport studies were performed on **1**–**4** employing the Mechanically Controlled Break-Junction (MCBJ) technique using a home-built set-up.[51,52] The MCBJ technique relies on a three-point bending mechanism allowing for the repeated breaking and making of a lithographically defined gold nanowire on a flexible substrate. Molecules are introduced by means of dropcasting a molecular solution with one of the compounds dissolved in dichloromethane (DCM) on a MCBJ sample. For all compounds a concentration of 75 μM is used. During the procedure of breaking a junction, the conductance is tracked as a function of electrode displacement, until the electrical noise floor of the set-up is reached, after which the junction electrodes are fused and the breaking process is repeated. For the measurements a bias voltage of 100 mV is applied across the junction; they are performed under ambient conditions.

The breaking process of the wire can lead either to a tunneling (empty) junction or a molecular (non-tunneling) junction. The data analysis is performed using a trained neural network to distinguish between these two types of junctions.[53] After this distinction the two groups are separated further, and the molecular features are further classified using the clustering algorithm k-*means* $++$.[54] Figure 3 displays the two-dimensional (2D) histograms of the raw data and the non-tunneling features as classes 1 and 2 as well as the tunneling classes. From all classes 1 it can be denoted that **1**–**4** form molecular junctions leading to plateau-like features in the 2D histogram. **2** shows a flat plateau with a narrow count distribution, whereas the classes 1 of **1**,**3** and **4**, are more slanted, indicating that **2** forms more stable molecular junctions. Classes 2 show broader features without a clear indication of plateau-like features for **1**,**2** and **4**, whereas **3** does not show this feature. Accompanying the 2D histograms of classes 1: Figure 4 shows the computed one-dimensional (1D) conductance histograms. Here, Figure 4a) shows the 1D histograms of **1** and **2**, whilst Figure 4b) shows the 1D histograms of **3** and **4**. The molecular conductance features of the 1D histograms are fitted with a Gaussian curve for which the peak defines the most probable conductance of a particular class. Comparing the values for **1** and **2**, found from Figure 4a) in red and green, we find a difference of about a factor of four; the values are $4.6\cdot10^{-7}\pm3.1\cdot10^{-7}$ G_0 and $2.1\cdot10^{-6}\pm1.1\cdot10^{-6}$ G_0, respectively. These low conductance values were expected as all channels comprise a central *meta*-benzene corner. The larger value recorded for **2** probably

Research Article
doi.org/10.1002/ejoc.202400914

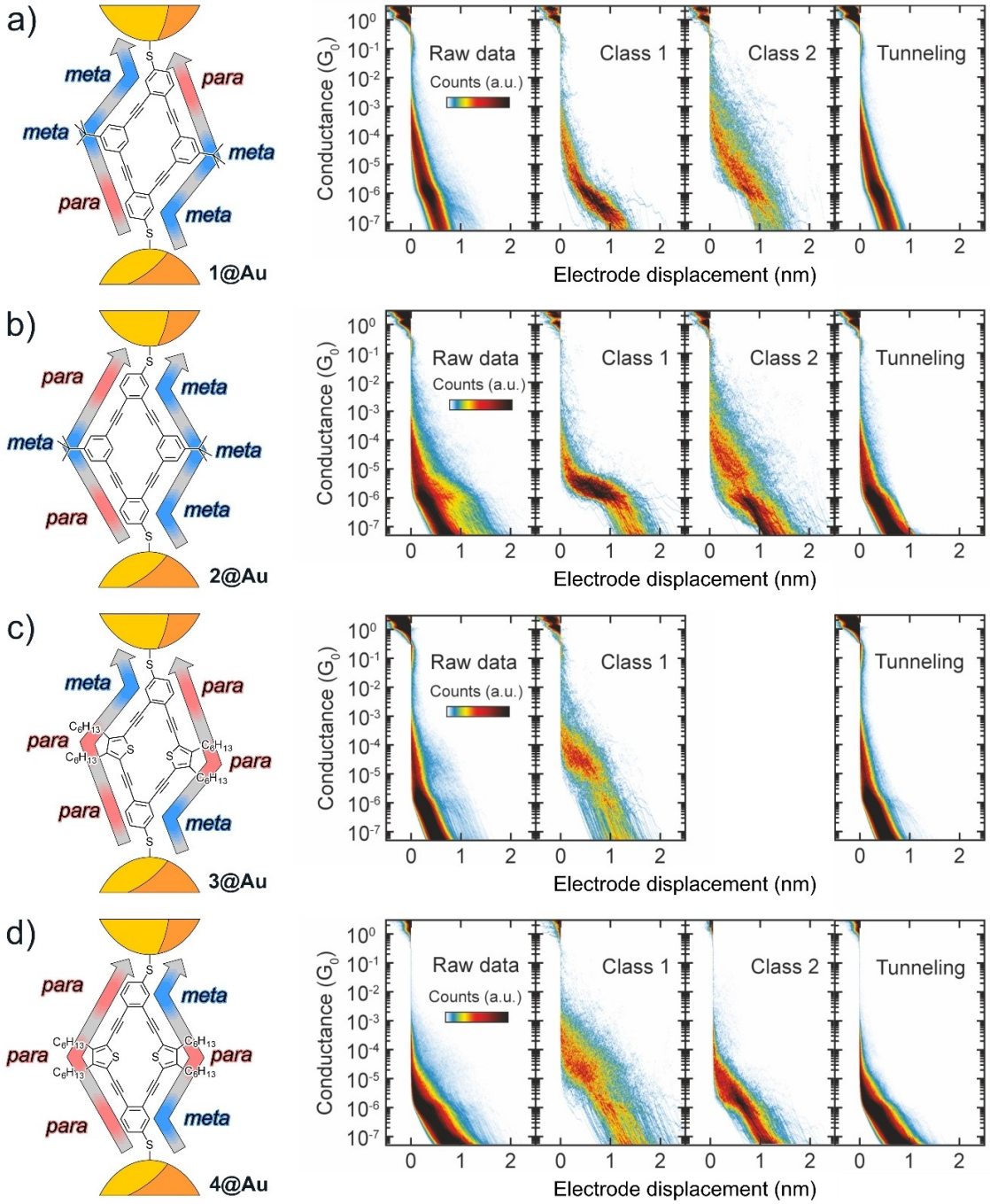

Figure 3. Sketch of the molecular junctions with grey arrows displaying the transport channels and two-dimensional (2D) conductance vs. electrode displacement histograms of: from the left to the right: the raw data, and the non-tunneling classes and tunneling class obtained from the data analysis using a Neural Network and the clustering algorithm k-means++, for which the latter a region of interest between [0,2.5] nm and [$10^{-0.5}$, $10^{-7.0}$] is used (see main text) for **a) 1**, **b) 2**, **c) 3**, and **d) 4**. Note that for the junctions with macrocycle **3** only one non-tunneling class has been found. Raw data histograms are constructed of 10000 consecutive traces for of **a)**, **c)** and **d)**, and 5000 consecutive traces in the case of **b)**.

reflects the superior transport features of the left channel with *para*-connections to both anchor groups and only the central *meta*-connection as bottle neck. Interestingly, the similar one-pathway structure, the acetyl masked 4,4′-(1,3-phenylenebis(ethyne-2,1-diyl))dibenzenethiol (labeled as *meta*-OPE3-SAc) has been reported in a similar experimental set-up with a conductance of about $3.2 \cdot 10^{-6}$ G_0.[21] It thus seems that the presence of a second, less favorable transport channel in the macrocycle **2** reduces the conductance of the entire system. A similar phenomenon has been reported for transient molecular junctions in an STM break junction experiment investigating compact tolane model compounds decorated with additional bis-ethynyl [*cis*-$Pt(PEt_3)_2]^{2+}$ bridges. The recorded single molecule conductance dropped significantly with every Pt-

Research Article
doi.org/10.1002/ejoc.202400914

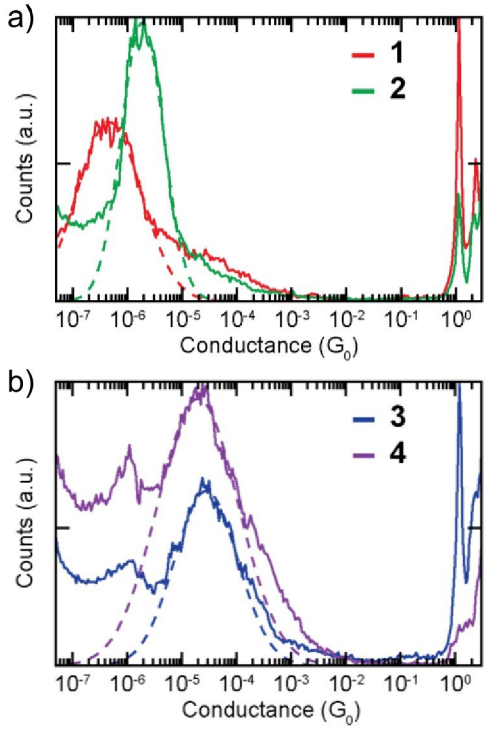

Figure 4. Corresponding one-dimensional (1D) conductance histograms to the classes 1 of the 2D histograms for **a) 1** and **2**, and **b) 3** and **4**. The peak in the 1D histograms around 10^{-6} G_0 is due to an artefact in the measurement system, as described in ref. [52].

bridge added.[44] The theoretical analysis not only suggested that all channels participate in electron transport, but also that the Pt-bridges contribute dominantly to the conductive orbitals, in spite of their poor transparency. In a similar manner the electronic transparency of the macrocycle **2** might reflect a superposition of both transport channels, the better conducting one on the left side with *para-meta-para* connections and the poor one on the right side with *meta-meta-meta* connections.

To increase the conductance of the macrocycles, the limiting central *meta*-connections, the 1,3-benzene subunits, were replaced by 2,5-thiophene subunits as *para*-connections. And indeed, with conductance values of $2.8 \cdot 10^{-5} \pm 2.7 \cdot 10^{-5}$ G_0 and $2.0 \cdot 10^{-5} \pm 1.9 \cdot 10^{-5}$ G_0, found from Figure 4b) in blue and purple, for **3** and **4** respectively, the transparency of the macrocycles increased by more than an order of magnitude. The recorded single molecule conductance values are not only very comparable, the left all *para*-channel of **4** does not outplay the conductance of the two similar channels of **3**. Only considering the connections of the aromatic subunits one would expect for each channel of **3** a value in the order of *meta*-OPE3-SAc, which also comprises two *para* and one *meta* connection. The recorded conductance of **3** is more than eight times larger than the value reported for *meta*-OPE3-SAc, suggesting that the combination of both channels in the macrocycle is more than the simple sum of both contributions. It must be mentioned that the conductance through heterocycles compared to *para* connected benzene can be influenced by the heteroatom effect.[58] It has also been shown that the lower aromaticity of thiophene compared to benzene leads to higher electron delocalization which results in a generally higher conductance.[59] However, when comparing results from reported conductance measurements of *para*-OPE-SAc and 2,5-substituted thiophene analogues, very comparable values were observed.[58,60]

Furthermore, the average length of each plateau-like feature has been analyzed. The lengths of the molecular plateaus of classes 1 are around 1 nm, without clear outliers, as the values are observed at: 1.1 nm, 1.2 nm, 0.9 nm and 1.2 nm for **1**–**4**, respectively. After adding a snapback of the gold electrodes upon breaking of the gold nanowire of about 0.5 nm,[55] these values are comparable to the sulfur-to-sulfur distances of the macrocycles which are in the order of 1.6–1.7 nm, as determined form the solid-state structure of **1** (1.75 nm) and estimated by MM2 based modelling of **2** (1.63 nm), **3** (1.72 nm), and **4** (1.70 nm) respectively.

Conclusions

The synthesis of the macrocyclic target structures **1** – **4** is reported. In particular the thiophene containing macrocycles **3** and **4** required the adaption of the thiophenol's protection group. 2-(4-Pyridinyl)ethyl turned out to be the protection group of choice providing access to **3** and **4**. The macrocyclizations based on *Sonogashira* cross-coupling reactions were less efficient for the thiophene comprising macrocycles **11b-c** and **12b-c** compared to their benzene analogues **11a** and **12a**. The presence of the coordinating ethyl pyridine protection group further reduced the macrocyclization yield of **11c** and **12c**. However, the yields were not only good enough to isolate and fully characterize the target structures, but also to provide samples for single-molecule transport investigations.

Proof-of-concept charge transport studies by employing the MCBJ technique revealed the suitability of these macrocycles for single-molecule transport experiments. These preliminary transport studies further unraveled i) the substantial increase in electronic transparency by replacing a *meta*-corner unit (1,3-diyl-benzene) by a 2,5-diyl-thiophene unit and ii) that both transport channels of these macrocyclic model compounds contribute to the over-all conductance in a more complex manner than just adding up.

We are currently exploring the manipulation of individual transport channels in order to investigate systematically the channels interplay resulting in the over-all conductance.

Supporting Information Summary

The synthetic protocols of all new compounds, their full characterization as well as their spectra are provided in the supporting information. The authors have cited the additional references[56] and[57] in the Supporting Information. The crystallographic data for **1** can be found under deposition number 2385394. These data are provided by the joint Cambridge Crystallographic Data Centre and Fachinformations zentrum

Karlsruhe Access Structures service www.ccdc.cam.ac.uk/structures.

Acknowledgements

A. G., L. O., H. S. J. v. d. Z., and M. M. acknowledge funding from the EC H2020 FET Open project grant agreement number 767187 "QuIET". The «van der Zant» group acknowledges support from the Dutch funding agency, NWO. The «Mayor» group acknowledges generous support by the Swiss National Science Foundation (200020_207744). M.M. acknowledges support from the 111 project (Grant No. 90002-18011002). Open Access funding provided by Universität Basel is acknowledged. Open Access funding enabled and organized by Projekt DEAL.

Conflict of Interests

The authors declare no conflict of interest.

Data Availability Statement

The data that support the findings of this study are available in the supplementary material of this article.

Keywords: Strained macrocycle · Interference · Mechanically controlled break junctions · Substitution pattern · Parallel pathways

[1] S. V. Aradhya, L. Venkataraman, *Nat. Nanotechnol.* **2013**, *8*, 399.
[2] T. A. Su, M. Neupane, M. L. Steigerwald, L. Venkataraman, C. Nuckolls, *Nat. Rev. Mater.* **2016**, *1*, 1.
[3] J. Liu, X. Huang, F. Wang, W. Hong, *Acc. Chem. Res.* **2019**, *52*, 151.
[4] F. Schwarz, E. Lörtscher, *J. Phys. Condens. Matter* **2014**, *26*, 474201.
[5] W.-Y. Lo, N. Zhang, Z. Cai, L. Li, L. Yu, *Acc. Chem. Res.* **2016**, *49*, 1852.
[6] X. Li, Z. Tan, X. Huang, J. Bai, J. Liu, W. Hong, *J. Mater. Chem. C* **2019**, *7*, 12790.
[7] L. J. O'Driscoll, M. R. Bryce, *Nanoscale* **2021**, *13*, 1103.
[8] L. J. O'Driscoll, M. R. Bryce, *Nanoscale* **2021**, *13*, 10668.
[9] A. Aggarwal, V. Kaliginedi, P. K. Maiti, *Nano Lett.* **2021**, *21*, 8532.
[10] S.-X. Liu, A. K. Ismael, A. Al-Jobory, C. J. Lambert, *Acc. Chem. Res.* **2023**, *56*, 322.
[11] C. M. Guédon, H. Valkenier, T. Markussen, K. S. Thygesen, J. C. Hummelen, S. J. Van Der Molen, *Nat. Nanotechnol.* **2012**, *7*, 305.
[12] D. Z. Manrique, C. Huang, M. Baghernejad, X. Zhao, O. A. Al-Owaedi, H. Sadeghi, V. Kaliginedi, W. Hong, M. Gulcur, T. Wandlowski, M. R. Bryce, C. J. Lambert, *Nat. Commun.* **2015**, *6*, 6389.
[13] T. Hansen, G. C. Solomon, D. Q. Andrews, M. A. Ratner, *J. Chem. Phys.* **2009**, *131*, 194704.
[14] G. C. Solomon, D. Q. Andrews, T. Hansen, R. H. Goldsmith, M. R. Wasielewski, R. P. Van Duyne, M. A. Ratner, *J. Chem. Phys.* **2008**, *129*, 054701.
[15] T. Tada, K. Yoshizawa, *Phys. Chem. Chem. Phys.* **2015**, *17*, 32099.
[16] G. C. Solomon, C. Herrmann, T. Hansen, V. Mujica, M. A. Ratner, *Nat. Chem.* **2010**, *2*, 223.
[17] C. R. Arroyo, S. Tarkuc, R. Frisenda, J. S. Seldenthuis, C. H. M. Woerde, R. Eelkema, F. C. Grozema, H. S. J. van der Zant, *Angew. Chem. Int. Ed.* **2013**, *52*, 3152.
[18] T. Markussen, R. Stadler, K. S. Thygesen, *Nano Lett.* **2010**, *10*, 4260.
[19] S. V. Aradhya, J. S. Meisner, M. Krikorian, S. Ahn, R. Parameswaran, M. L. Steigerwald, C. Nuckolls, L. Venkataraman, *Nano Lett.* **2012**, *12*, 1643.
[20] R. Frisenda, V. A. E. C. Janssen, F. C. Grozema, H. S. J. van der Zant, N. Renaud, *Nat. Chem.* **2016**, *8*, 1099.
[21] X. Liu, S. Sangtarash, D. Reber, D. Zhang, H. Sadeghi, J. Shi, Z. Xiao, W. Hong, C. J. Lambert, S. Liu, *Angew. Chem. Int. Ed Engl.* **2017**, *56*, 173.
[22] S. Ballmann, R. Härtle, P. B. Coto, M. Elbing, M. Mayor, M. R. Bryce, M. Thoss, H. B. Weber, *Phys. Rev. Lett.* **2012**, *109*, 056801.
[23] M. L. Perrin, R. Frisenda, M. Koole, J. S. Seldenthuis, J. A. C. Gil, H. Valkenier, J. C. Hummelen, N. Renaud, F. C. Grozema, J. M. Thijssen, D. Dulić, H. S. J. van der Zant, *Nat. Nanotechnol.* **2014**, *9*, 830.
[24] D. Fracasso, H. Valkenier, J. C. Hummelen, G. C. Solomon, R. C. Chiechi, *J. Am. Chem. Soc.* **2011**, *133*, 9556.
[25] G. C. Solomon, D. Q. Andrews, R. P. Van Duyne, M. A. Ratner, *ChemPhysChem* **2009**, *10*, 257.
[26] M. H. Garner, H. Li, Y. Chen, T. A. Su, Z. Shangguan, D. W. Paley, T. Liu, F. Ng, H. Li, S. Xiao, C. Nuckolls, L. Venkataraman, G. C. Solomon, *Nature* **2018**, *558*, 415.
[27] H. Vazquez, R. Skouta, S. Schneebeli, M. Kamenetska, R. Breslow, L. Venkataraman, M. S. Hybertsen, *Nat. Nanotechnol.* **2012**, *7*, 663.
[28] C. A. Perroni, D. Ninno, V. Cataudella, *J. Phys. Condens. Matter* **2016**, *28*, 373001.
[29] J. P. Bergfield, M. A. Solis, C. A. Stafford, *ACS Nano* **2010**, *4*, 5314.
[30] R. Miao, H. Xu, M. Skripnik, L. Cui, K. Wang, K. G. L. Pedersen, M. Leijnse, F. Pauly, K. Wärnmark, E. Meyhofer, P. Reddy, H. Linke, *Nano Lett.* **2018**, *18*, 5666.
[31] V. Kaliginedi, P. Moreno-García, H. Valkenier, W. Hong, V. M. García-Suárez, P. Buiter, J. L. H. Otten, J. C. Hummelen, C. J. Lambert, T. Wandlowski, *J. Am. Chem. Soc.* **2012**, *134*, 5262.
[32] N. Darwish, I. Díez-Pérez, P. Da Silva, N. Tao, J. J. Gooding, M. N. Paddon-Row, *Angew. Chem. Int. Ed.* **2012**, *51*, 3203.
[33] K. Reznikova, C. Hsu, W. M. Schosser, A. Gallego, K. Beltako, F. Pauly, H. S. J. van der Zant, M. Mayor, *J. Am. Chem. Soc.* **2021**, *143*, 13944.
[34] D. Stefani, K. J. Weiland, M. Skripnik, C. Hsu, M. L. Perrin, M. Mayor, F. Pauly, H. S. J. van der Zant, *Nano Lett.* **2018**, *18*, 5981.
[35] P. Zwick, C. Hsu, M. El Abbassi, O. Fuhr, D. Fenske, D. Dulić, H. S. J. van der Zant, M. Mayor, *J. Org. Chem.* **2020**, *85*, 15072.
[36] W. M. Schosser, C. Hsu, P. Zwick, K. Beltako, D. Dulić, M. Mayor, H. S. J. van der Zant, F. Pauly, *Nanoscale* **2022**, *14*, 984.
[37] Y. Aharonov, D. Bohm, *Phys. Rev.* **1959**, *115*, 485.
[38] H. Batelaan, A. Tonomura, *Phys. Today* **2009**, *62*, 38.
[39] R. A. Webb, S. Washburn, C. P. Umbach, R. B. Laibowitz, *Phys. Rev. Lett.* **1985**, *54*, 2696.
[40] M. Mayor, H. B. Weber, J. Reichert, M. Elbing, C. von Hänisch, D. Beckmann, M. Fischer, *Angew. Chem. Int. Ed.* **2003**, *42*, 5834.
[41] M. Kiguchi, H. Nakamura, Y. Takahashi, T. Takahashi, T. Ohto, *J. Phys. Chem. C* **2010**, *114*, 22254.
[42] K. Yoshizawa, *Acc. Chem. Res.* **2012**, *45*, 1612.
[43] H. Chen, H. Zheng, C. Hu, K. Cai, Y. Jiao, L. Zhang, F. Jiang, I. Roy, Y. Qiu, D. Shen, Y. Feng, F. M. Alsubaie, H. Guo, W. Hong, J. F. Stoddart, *Matter* **2020**, *2*, 378.
[44] P. Duan, K. Qu, J.-Y. Wang, B. Zeng, C. Tang, H.-F. Su, Q.-C. Zhang, W. Hong, Z.-N. Chen, *Cell Rep. Phys. Sci.* **2021**, *2*, 100342.
[45] E. Leary, L. A. Zotti, D. Miguel, I. R. Márquez, L. Palomino-Ruiz, J. M. Cuerva, G. Rubio-Bollinger, M. T. Gonzales, N. Agrait, *J. Phys. Chem. C* **2018**, *122*(6), 3211–3218.
[46] G. D. Probst, S. Bowers, J. M. Sealy, B. Stupi, D. Dressen, B. M. Jagodzinska, J. Aquino, A. Gailunas, A. P. Truong, L. Tso, Y.-Z. Xu, R. K. Hom, V. John, J. S. Tung, M. A. Pleiss, J. A. Tucker, A. W. Konradi, H. L. Sham, J. Jagodzinski, G. Toth, E. Brecht, N. Yao, H. Pan, M. Lin, D. R. Artis, L. Ruslim, M. P. Bova, S. Sinha, T. A. Yednock, S. Gauby, W. Zmolek, K. P. Quinn, J.-M. Sauer, *Bioorg. Med. Chem. Lett.* **2010**, *20*, 6034.
[47] J. Grolleau, P. Frère, F. Gohier, *Synthesis* **2015**, *47*, 3901.
[48] C. J. Yu, Y. Chong, J. F. Kayyem, M. Gozin, *J. Org. Chem.* **1999**, *64*, 2070.
[49] J. P. Collman, M. Zhong, S. Costanzo, C. J. Sunderland, A. Aukauloo, K. Berg, L. Zeng, *Synthesis* **2001**, *2001*, 0367.
[50] A. R. Katritzky, G. R. Khan, O. A. Schwarz, *Tetrahedron Lett.* **1984**, *25*, 1223.
[51] C. A. Martin, R. H. M. Smit, R. van Egmond, H. S. J. van der Zant, J. M. van Ruitenbeek, *Rev. Sci. Instrum.* **2011**, *82*, 053907.
[52] L. Ornago, *Complexity of Electron Transport in Nanoscale Molecular Junctions*, Ph.D. Thesis, (TU Delft), **2023**, 125 p. (Casimir PhD Series; 4). doi: 10.4233/uuid:e6002163-58f0-48e1-bce2-02ac111a8adf.
[53] F. Van Veen, L. Ornago, H. S. J. Van Der Zant, M. El Abbassi, *J. Mater. Chem. C* **2023**, DOI: 10.1039.D3TC02346J.
[54] D. Cabosart, M. El Abbassi, D. Stefani, R. Frisenda, M. Calame, H. S. J. van der Zant, M. L. Perrin, *Appl. Phys. Lett.* **2019**, *114*, 143102.

[55] C. Huang, A. V. Rudnev, W. Hong, T. Wandlowski, *Chem. Soc. Rev.* **2015**, *44*, 889.
[56] in the SI: D. L. Comins, J. D. Brown, *JOC* **1984**, *49*, 1078.
[57] in the SI: G. D. Probst, S. Bowers, J. M. Sealy, B. Stupi, D. Dressen, B. M. Jagodzinska, J. Aquino, A. Gailunas, A. P. Truong, L. Tso, Y.-Z. Xu, R. K. Hom, V. John, J. S. Tung, M. A. Pleiss, J. A. Tucker, A. W. Konradi, H. L. Sham, J. Jagodzinski, G. Toth, E. Brecht, N. Yao, H. Pan, M. Lin, D. R. Artis, L. Ruslim, M. P. Bova, S. Sinha, T. A. Yednock, S. Gauby, W. Zmolek, K. P. Quinn, J.-M. Sauer, *Bioorg. Med. Chem. Lett.* **2010**, *20*, 6034.
[58] X. Liu, S. Sangtarash, D. Reber, D. Zhang, H. Sadeghi, J. Shi, Z. Xiao, W. Hong, C. J. Lambert, S. Liu, *Angew. Chem. Int. Ed.* **2017**, *129*(1), 179–182.
[59] W. Chen, H. Li, J. R. Widawsky, C. Appayee, L. Venkataraman, R. Breslow, *J. Am. Chem. Soc.* **2014**, *136*(3), 918–920.
[60] M. Naher, E. Gorenskaia, S. A. Moggach, T. Becker, R. J. Nichols, C. J. Lambert, P. J. Low, *Aust. J. Chem.* **2022**, *75*(9), 506–522.

Manuscript received: August 8, 2024
Revised manuscript received: October 7, 2024
Accepted manuscript online: November 6, 2024
Version of record online: November 21, 2024